# Spring-time enhancement in aerosol burden over a high-altitude location in western trans-Himalaya: results from long-term observations

**Sobhan Kumar Kompalli[1], S. Suresh Babu[1,*], Lakshmi N. Bharatan[1] and K. Krishna Moorthy[2,3]**

[1]Space Physics Laboratory, Vikram Sarabhai Space Centre, Thiruvananthapuram 695 022, India
[2]ISRO Head Quarters, Bengaluru 560 231, India
[3]Present address: Centre for Atmospheric and Oceanic Sciences, Indian Institute of Science, Bengaluru 560 012, India

**Long-term measurements (from August 2009 to December 2014) of aerosol black carbon mass concentration ($M_{BC}$) and spectral aerosol optical depth (AOD) were carried out from a high-altitude location, Hanle in western trans-Himalaya as part of the Regional Aerosol Warming Experiment. Both $M_{BC}$ and AOD showed distinct annual pattern with a clear spring-time enhancement (April–June) with significant inter-annual variability associated with the changes in source processes. The potential source regions contributing to the spring-time enhancement in aerosol loading are the dust-dominated west Asian region as well as biomass burning from NW India. The overall annual mean value of $M_{BC}$ over Hanle is extremely low compared to many other Himalayan locations, including the Ganges Valley Aerosol Experiment campaign site at Nainital, which also showed spring-time (pre-monsoon) enhancement. The vertical extents of elevated aerosol layers, which contribute to the spring-time enhancement, are found to be in the range 5–7 km amsl from the analysis of vertical profiles of extinction coefficients from CALIPSO data.**

**Keywords:** Aerosol optical depth, black carbon, spring-time enhancement, high-altitude locations.

## Introduction

THE important role of aerosols in various atmospheric processes that affect the Earth's radiation balance is well recognized. The recent Intergovernmental Panel for Climate Change (IPCC) report[1] has pointed out that the total radiative forcing due to aerosols (both direct and cloud adjustments due to aerosols) is –0.9 (–1.9 to –0.1 W m$^{-2}$). While most of the aerosols result in a negative forcing (cooling), the absorbing black carbon (BC) aerosols contribute to warming effect[2,3]. One of the difficulties in the quantification of aerosol radiative forcing arises due to the high spatio-temporal variability of aerosol properties. With lifetimes of the order of days to weeks, aerosols may be transported over long distances and reach distant locations, especially in dry conditions and in the absence of precipitation which results in slower scavenging from the atmosphere. This warrants for region-specific aerosol observations which aim at the characterization of regional hotspots, background levels and transport pathways both vertically and horizontally. One of the better ways to understand the regional background features and to delineate the influence of regional sources and long-range transport is through long-term measurements from high-altitude remote locations devoid of significant local anthropogenic sources. Observations from high-altitude locations have global relevance in understanding the free-tropospheric background conditions. Such observations over South Asia in general and the Indian region in particular are highly relevant due to the increasing anthropogenic emissions, their strong impact on the hydrological cycle[4], Indian/Asian summer monsoon[5,6], and as a potential health hazard to the large population (~1.3 billion) residing in this region. The Himalayan mountain range forms a natural orographic barrier to the northward transport of pollutants resulting in the build-up of aerosols over the Indo-Gangetic Plains (IGP). The regional as well long-range transport of aerosols to the remote Himalayan locations may have substantial effect on regional climate change[5,7,8]. The tropospheric warming caused by the absorbing aerosols over the Himalaya is important due to its role in influencing the middle–upper tropospheric temperature gradient between the Himalaya–Tibetan Plateau and the oceanic region to the south, which controls the onset of the Asian monsoon[9,10]. Lau *et al.*[5] demonstrated the role of dust (mixed with BC) aerosols on the enhanced heating at elevated levels over northern India, the foothills of the Himalaya and Tibetan Plateau, leading to the strengthening of the meridional tropospheric temperature gradient

*For correspondence. (e-mail: s_sureshbabu@vssc.gov.in)

and consequent influence on monsoon rainfall. Bollasina *et al.*[9] showed a link between high loads of absorbing aerosols and deficient spring-time precipitation through regression of rainfall on aerosol index (AI), and attributed it to dissipation of clouds through the aerosol semi-direct effect. Thus long-term measurements from such high-altitude remote locations not only help in addressing the pertinent issues described above, but are also useful to delineate the ever-growing human impact in this region on the background conditions and to suggest potential mitigation strategies. In spite of BC over the Himalaya being a topic of major scientific interest, there is limited availability of long-term data, especially over the western and southern slopes of the Himalaya. A number of field experiments have been devised for aerosol measurements in the Himalayan region[5,11–17]. The observational evidence of the persistent elevated aerosol layers over the Indian region and the northward gradient in atmospheric warming due to such layers, which was unravelled during the multi-platform field experiment 'Integrated Campaign for Aerosols, gases and Radiation Budget (ICARB)'[18,19], led to the formation of Regional Aerosol Warming EXperiment (RAWEX) under the Indian Space Research Organisation Geosphere Biosphere Program (ISRO-GBP)[20]. One of the important objectives of RAWEX is the quantification of amplitude, frequency of occurrence, seasonal trends of elevated aerosols and atmospheric warming caused by them over the Indian region, and also to delineate the share of long-range transport and local contributions to this phenomenon. The Ganges Valley Aerosol Experiment (GVAX) was a multi-institution, multi-instrument campaign aimed at the detailed understanding of the physical, optical and radiative properties of atmospheric aerosols over the Gangetic–Himalayan (GH) region[21,22], by carrying out intense observations over Manora Peak (29.4°N, 79.5°E, 1958 m amsl), Nainital (located in the Central Himalaya) using the ARM Mobile Facility (AMF) for a 10-month period during June 2011–March 2012. One of the stated objectives of GVAX is to understand the effect of aerosol heating due to increase in the mid-tropospheric aerosols over the GH region on Indian summer monsoon[22]. In view of the overlapping scientific interest, joint RAWEX–GVAX experiments were initiated under ISRO-GBP.

As part of RAWEX, a high-altitude aerosol observatory has been established over western Himalaya, at Hanle (32.5°N, 78.5°E and 4520 m amsl) in August 2009. This observatory is also a part of the network of observatories under Aerosol Radiative Forcing over India (ARFI) project of ISRO-GBP, which is now known as ARFINET[23,24]. Some of the findings from this observatory have been published earlier[25–31]. These include the role of photochemistry in the new particle formation events at the free-tropospheric altitudes[25], temporal evolution and annual cycle in BC concentration over the Himalaya[26], dust transport and associated changes in physical and optical properties of aerosols[27–31] and spring-time enhancement in aerosol optical depth (AOD) and BC over Hanle[30]. While these earlier works are focused on characterization of aerosol optical and physical properties over Hanle, this article presents the quantitative estimation of spring-time enhancement in aerosol loading, its vertical structure and possible reasons for the inter-annual variability in spring-time enhancement based on long-term observations of aerosol properties over Hanle during August 2009–December 2014. This is the only aerosol observatory in this region that provides continuous measurements of various aerosol parameters from such an altitude level. Uniqueness of the database from this free-tropospheric location has been exploited to understand the influence of long-range transport and regional sources in determining the observed variability in aerosol loading over the region.

## Measurements

### *Location and local meteorology*

The experimental location, Hanle is situated in the western trans-Himalaya in Ladakh region, Jammu and Kashmir, India, and to the southwest of the Tibetan plateau (Figure 1). This is a remote, near-free-tropospheric location, far from any major industrial activities and devoid of any local anthropogenic sources. Meteorologically, this location is akin to a high-altitude 'cold desert' environment with dry conditions (annual precipitation <10 cm), sparse seasonal vegetation (very little shrubs) and clear skies which prompted the establishment of the 2 m Himalayan Chandra Telescope (HCT) for astronomical observations by the Indian Institute of Astrophysics, Bengaluru. The aerosol measurement site is near this telescope facility and located atop Mt. Saraswati ~300 m above the surrounding valley region which consists of a base camp and Hanle village. There are several mountain peaks of the Zanskar and Ladakh ranges around the observatory (some of which are even taller than Mt. Saraswati), among which some are snow-covered throughout the year while others experience seasonal precipitation, especially during winter (December–February) and summer (July–August). More details of this near-free-tropospheric background location are available in the literature[25–31].

Figure 2 shows the prevailing surface meteorological conditions obtained using data from a collocated automatic weather station. The top panel of Figure 2 *a–d* shows monthly means temperature (°C), pressure (hPa), relative humidity (RH; %) and wind speed (m $s^{-1}$) considering data for the five-year period (2009–14) and vertical bars represent the corresponding standard deviations. The air temperature exhibits a strong seasonality, with higher (~10–15°C) temperatures during July–August and lower ones during December–January (≃15°C to –10°C).

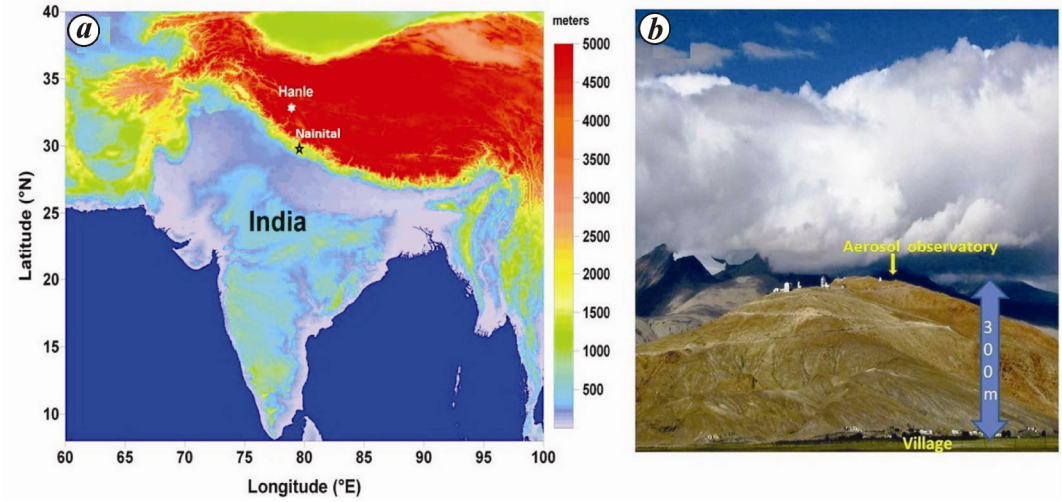


**Figure 1.** ***a***, Geographic location of Hanle (marked by a star), Ladakh, India on the topographic map. ***b***, Aerosol observatory located on the mountain top at Hanle. Nainital, the location where the GVAX campaign was conducted is also marked.

The monthly mean RH values ranging between 25% and 50% indicate the dry nature of the location throughout the year. The monthly mean wind speed varies between 3 and 7 m $s^{-1}$ with large standard deviation in all the months, and daily mean values occasionally reaching as high as 20 m $s^{-1}$, suggesting windy conditions. The whole year is divided into four season, namely winter (December to February), spring (March to June), summer (July to September) and autumn (October and November). The bottom panel of Figure 2 shows the polar diagram of hourly mean wind speeds and directions in different seasons. As evident from the figure, the station predominantly experiences winds coming from southwesterly to southerly directions, which are sparsely inhabited parts, and infrequent and weak winds arrive from the east or west direction.

## *Data*

The long-term observations of aerosol BC and spectral AOD carried out during the period August 2009–December 2014 (65 months), one of the strongest databases from the high-altitude western Himalayan region, have been used in the present study. Continuous measurements of BC mass concentration ($M_{BC}$) have been carried using a two-channel (370 and 880 nm) aethalometer (make: Magee Scientific)[26,30]. The Aethalometer works on the principle of optical attenuation, in which continuous filtration of the particles through a quartz filter tape that is illuminated by light sources is utilized, and light attenuation between consecutive measurements is used for the estimation of $M_{BC}$ deposited on the filter tape during this sampling period. We have considered attenuation at the wavelength of 880 nm for the estimation of $M_{BC}$. Since the ambient pressure level at Hanle (~590 hPa) is lower than mean sea level, an additional external pump is used to maintain constant mass flow rate of 6 lpm (litres per minute). Sampling has been carried out with a time base of 5 min by the continuous aspiration of ambient air through an inlet tube from a height of ~5 m above the ground. In order to avoid possible obstruction to the measurements that can arise due to condensation of water in the sampling lines during the conditions with extremely low temperatures (especially in winters, when temperatures go down to as low as –20°C) and periods of high RH (due to precipitation), a heated inlet, maintained at a temperature of ~60°C, has been used. Since the mass flow rate of 6 lpm mentioned above for the instrument is under standard temperature ($T \sim 293$ K) and pressure ($P_0$ ~1013 hPa) conditions, the measured $M_{BC}$ values were corrected for lower ambient pressures using the following relation

$$M_{BC} = M^*_{BC}\left[\frac{P_0 T}{P T_0}\right]^{-1}, \quad (1)$$

where $M^*_{BC}$ is the instrument-measured raw mass concentration at ambient conditions, $P_0$ and $P$ are the standard and ambient pressures, and $T_0$ and $T$ are the corresponding temperatures. More details about the instrument, its uncertainties, and corrections applied to the data are described in detail by Babu *et al.*[26].

The spectral AOD at 10 wavelength bands centred at 380, 400, 450, 500, 600, 650, 750, 850, 935 and 1025 nm have been measured in all clear and partly clear sky days using the ground-based multi wavelength solar radiometer (MWR) instrument. This instrument, which utilizes the principle of filter-wheel radiometry to obtain spectral AOD following the Langley plot technique, is widely used across the ARFINET observatories. Recently, Babu *et al.*[24]

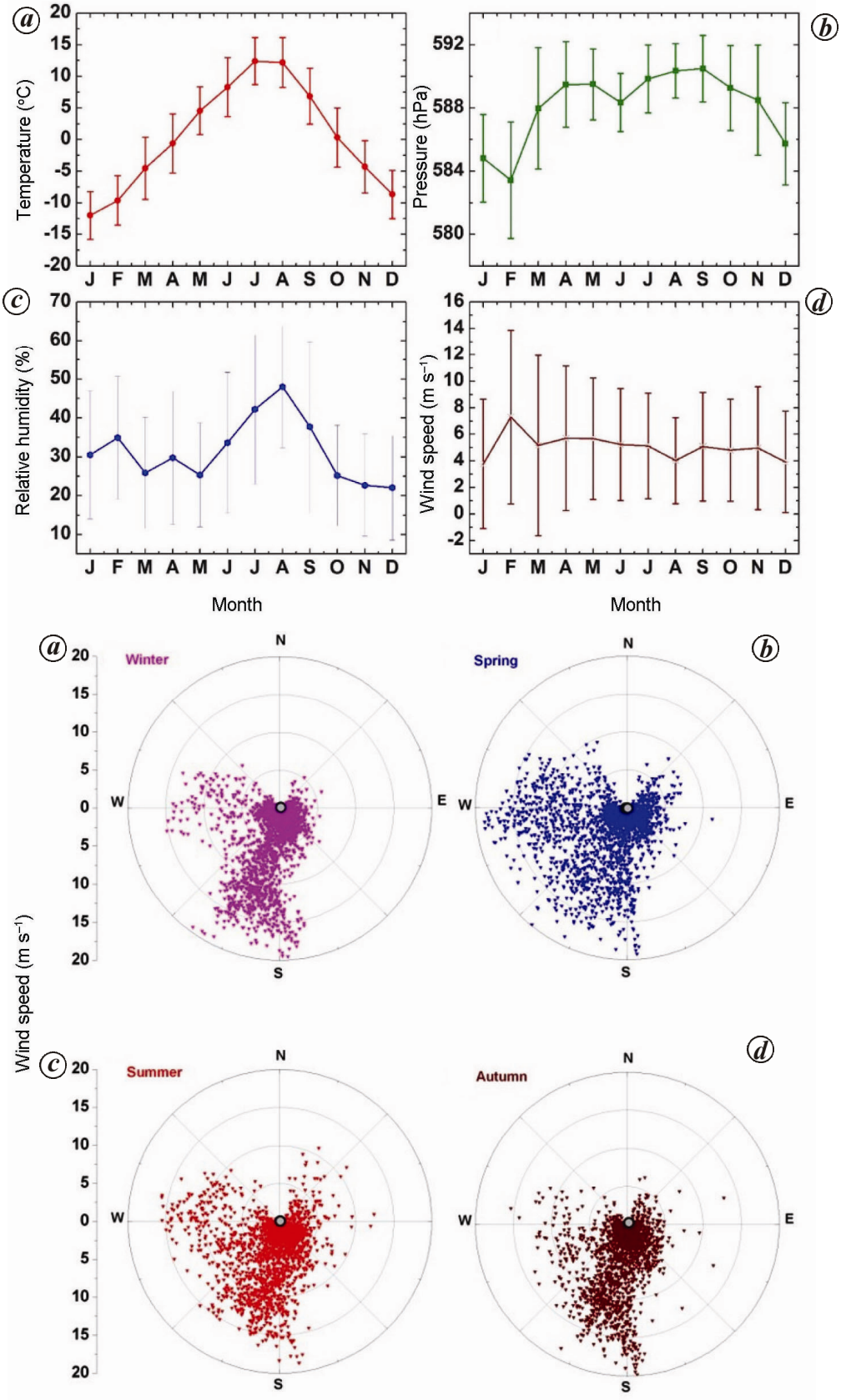


**Figure 2.** (Top panel) Annual variation of monthly mean air temperature (***a***), surface pressure (***b***) relative humidity (***c***) and wind speeds (***d***) at Hanle. Vertical lines are the standard deviation from the mean values. (Bottom panel): Polar diagrams showing distribution of surface winds during different seasons.

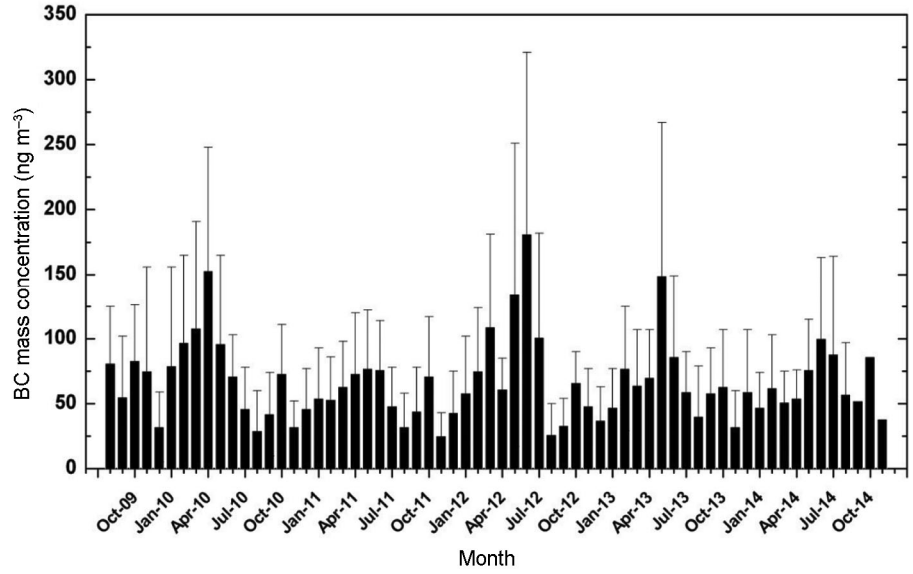


**Figure 3.** Temporal variation of monthly mean black carbon (BC) mass concentration ($M_{BC}$) for the period August 2009–December 2014. Vertical lines are the standard deviation.

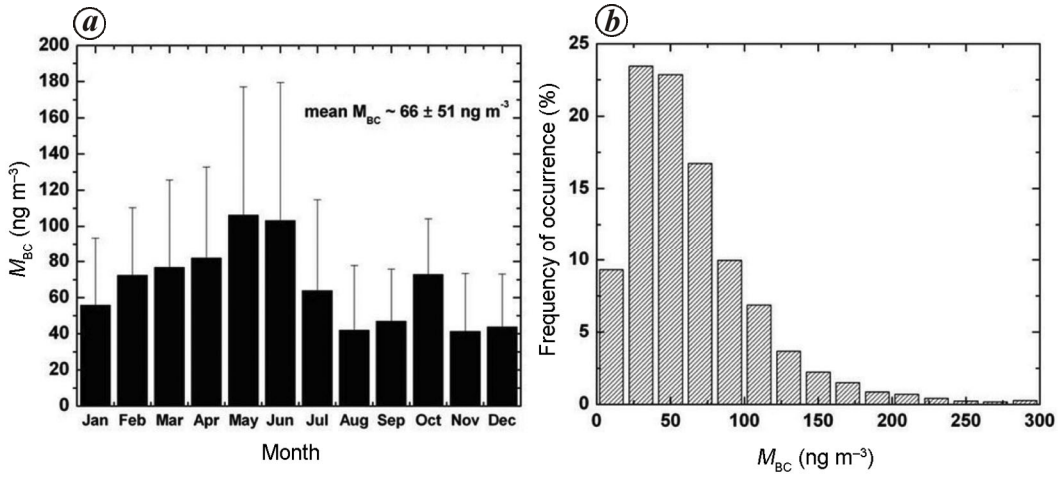


**Figure 4.** ***a***, Long-term annual pattern of monthly mean $M_{BC}$ considering the whole measurement period (August 2009–December 2014). ***b***, Frequency of occurrence of $M_{BC}$ for the same period.

have discussed long-term regional AOD trends over the Indian region using the database from the network of observatories equipped with MWR instruments. More details about this system, its data deduction methodology, error budgeting, and comparison of its performance with other instruments are extensively available in the literature[23,24,32].

## Results and discussion

### *Black carbon mass concentration*

Figure 3 shows the temporal variation of monthly mean $M_{BC}$ values with the vertical lines indicating the standard deviation. Overall, the monthly mean $M_{BC}$ values vary between ~25 and 175 ng m$^{-3}$, with the highest values seen during April–June (spring) and the lowest during August–September (summer). Clearly, the $M_{BC}$ values depict a systematic annual pattern that repeats each year with certain degree of inter-annual variability (this aspect is discussed in subsequent sections). As such, there is no discernable increasing or decreasing long-term trend in $M_{BC}$ over the measurement period.

Figure 4 *a* shows the long-term annual variation pattern considering the entire data. As is evident from the figure, there is a clear build-up of aerosol BC from winter (December–February) to spring (April–June). Subsequently, the $M_{BC}$ values drop to their lowest during summer (July–September) and a prominent second peak in $M_{BC}$ is seen in October (in all the years), which disappears by November. The frequency of distribution of $M_{BC}$

is skewed (Figure 4 *b*) and ~60% of the values remain below the long-term annual mean (~66 ± 51 ng m$^{-3}$). Almost 82% of the $M_{BC}$ values remains <100 ng m$^{-3}$, 15% is between 100–200 ng m$^{-3}$ and only close to 3% is greater than 200 ng m$^{-3}$. Higher $M_{BC}$ values are noticed predominantly during spring and preferably associated with the advection of westerly air-masses.

Figure 5 shows the annual mean $M_{BC}$ (~66 ± 51 ng m$^{-3}$) observed over Hanle along with the reported values from other Himalayan sites. The mean $M_{BC}$ observed over Hanle is the lowest (close to the value ~55 ng m$^{-3}$ reported over Muztagh Ata Mountain[33]; 38.28°N, 75.00°E, 4500 m amsl) among all the Indian Himalayan stations. Interestingly $M_{BC}$ value over Hanle is lower compared to that reported from the Nepal Climate Observatory–Pyramid (NCO-P)[34], despite Hanle being less elevated than NCO-P. This is due to the proximity of NCO–P to Kathmandu valley (~200 km away) and transport of pollutants to the station from Khumbu valley (which represents a natural chimney through which pollutants can be vented to NCO-P and the higher Himalaya) through thermal winds (mountain-valley breeze circulation)[34]. Notwithstanding the large differences in magnitude, the seasonal trends in the observed $M_{BC}$ at Hanle are quite similar to that in NCO-P. Table 1 provides a detailed comparison of $M_{BC}$ at Hanle with other high-altitude Himalayan locations[33–41]. Other stations are at a much lower elevation and less pristine compared to Hanle in view of the observed higher BC mass loading over these locations. Significant variability in $M_{BC}$ among various Himalayan stations (as seen in Figure 5) suggests that different parts of the Himalaya are influenced by distinct sources with varying strengths and transport pathways. The impact of transport at each site also depends on the time the airmasses spend over polluted upwind regions before they arrive at the receptor site (the aspects of long-range transport and strength of the potential source regions have been examined in detail in a later section). Another interesting aspect from Table 1 is that over some high-altitude stations, e.g. Darjeeling (27.04°N, 88.26°E; 2200 m amsl) $M_{BC}$ is higher than at stations at lower elevation. This is due to their proximity to urban centres and tourist destinations, which result in significant local emissions. Also, the nature of upwind regions which contribute to aerosol transport is another determining factor. Recently, Sarkar *et al.*[38] examined $M_{BC}$ over Darjeeling station, located in the eastern Himalaya in India, and pointed out the distinctiveness of the impact of aerosol transport over different parts of the Himalaya. Although aerosol transport through west/northwest air-masses is more frequent in dry periods over the Himalaya, its impact is much higher over the eastern Himalaya compared to the western and the central Himalayan stations. While the western/northwestern air-masses arriving at the central and western Himalaya pass through only parts of the IGP (western IGP), the eastern Himalaya encounters the air-masses which pass through major portions of polluted IGP, thus carrying more anthropogenic pollutants. This highlights that each of the Himalayan regions is characteristically distinct from other regions, suggesting that region-wise concerted efforts are necessary to understand the prevailing aerosol systems.

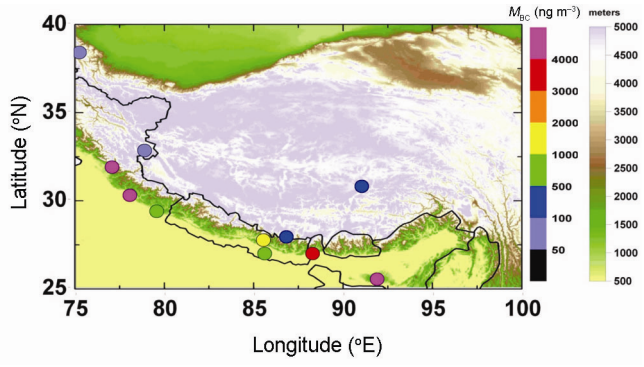


**Figure 5.** Comparison of annual mean $M_{BC}$ values reported from *in situ* measurements over other Himalayan locations.

The annual variation of BC is associated with source, sink strengths and regional as well as long-range transport pathways (in both vertical and horizontal directions). In remote locations such as Hanle, with apparently no local sources, the effectiveness of transport associated with synoptic circulation in bringing the pollutants from regional/long-distance sources (whose strength varies seasonally) determines the overall loading; while the mesoscale dynamics and prevailing meteorological conditions modulate these concentrations. During winter, low-level confinement of aerosols due to capping inversion associated with low temperatures, dry conditions and calm ambient winds prevailing over the adjoining plains (the northwestern IGP which is upwind to Hanle) and valleys result in lesser ventilation of the pollutants. These conditions, combined with prevailing synoptic low-level anti-cyclone over the entire Indian region, result in a reduced amount of transport of BC aerosols to the Himalayan region from the vastly populated IGP and the sub-Himalaya. With the advent of spring, increased insolation results in increased temperature and enhanced thermal convection which aid the effective transport of pollutants (both vertically and horizontally). In addition to such favourable circulation, longer lifetime of BC in free troposphere also contributes to the spring enhancement in $M_{BC}$. During summer, even though prevailing winds remain similar to those during spring (Figure 2), enhanced wet removal due to precipitation (below-cloud scavenging) as well as in-cloud scavenging due to prevailing large cloud cover result in decrease in $M_{BC}$ values during this season. These conditions disappear by autumn and $M_{BC}$ slightly increases compared to its summer value. Earlier Dumka *et al.*[15] have reported spring-time high $M_{BC}$ values over the central Himalayan site, Nainital

**Table 1.** Black carbon (BC) mass concentration (ng $m^{-3}$) at different locations over the Himalaya

| Location | Latitude and longitude | Altitude (m) | Annual mean BC mass concentration $M_{BC}$ (ng $m^{-3}$) |
|---|---|---|---|
| NCO–P[34] | 27.95N, 86.82E | 5079 | 160.5 |
| Nam Co[35] | 30.77N, 90.99E | 4730 | 127 |
| Hanle | 32.78N, 78.95E | 4520 | 66 ± 51 |
| Muztagh Ata[33] | 38.28N, 75.00E | 4500 | 55 |
| Qilian Mountain[36] | 39.5N, 96.51E | 4214 | 62 |
| Langtang, Nepal[37] | 28.13N, 85.60E | 3920 | 520 |
| Darjeeling[38] | 27.04N, 88.26E | 2200 | 3450 |
| Mukteshwar[13] | 29.43N, 79.61E | 2180 | 806 |
| Nagarkot[37] | 27.72N, 85.52E | 2150 | 1000 |
| Shillong[39] | 25.57N, 91.88E | 1965 | 5000 |
| Nainital[15] | 29.40N, 79.50E | 1958 | 825 |
| Kullu[40] | 31.90N, 77.10E | 1220 | 4600 |
| Dehradun[41] | 30.34N, 78.04E | 700 | 4400 |

(where subsequently the GVAX campaign has been conducted), which was attributed to lifting up of pollutants from the valley region by the convective boundary layer and increased local emissions. Apart from the difference in magnitudes, explicit difference in the annual pattern of $M_{BC}$ over Nainital and Hanle is seen in June and November. A drastic drop in $M_{BC}$ from preceding months was reported in June over Nainital (Figure 4; Dumka *et al.*[15]) owing to washout due to extensive rainfall, whereas over Hanle $M_{BC}$ values remained considerably high in June and dropped only in July, with the advent of summer. While the post-monsoon build-up of high $M_{BC}$ values over Nainital started in October and persisted in November as well (and continued till May), in the case of Hanle only October peak in $M_{BC}$ was noticeable, which disappeared by November.

## *Spring-time enhancement in black carbon*

In the present study, spring-time enhancement in aerosol BC loading has been noticed consistently in all the years. The spring-time enhancement over high-altitude free-tropospheric locations is a well-established feature noticed over several sites spread across the globe[42]. Andrews *et al.*[42] presented the climatology of aerosol optical properties based on long-term, *in situ* measurements over several high-altitude locations spread across the 20–50°N lat. band in the northern hemisphere. They observed that the amount of light absorption and scattering at such high-altitude sites either peaks in spring or it has a broad spring to summer enhancement. The reasons are attributed to the pollution outflow from upwind regions aided by stronger upslope transport and enhanced atmospheric boundary layer (ABL) heights flushing out the aerosols to higher altitudes through convective transport. Over the Himalaya also, strong westerlies associated with the Asian monsoon prevail during pre-monsoon. The airmasses having long continental overpass, pick up dust and carbonaceous aerosols from western and northwestern India and transport them to the IGP and the Himalaya. Several studies carried out from the other Himalayan locations suggest that biomass (agricultural) burning over the IGP and forest fires over the Himalayan foothills are one of the major sources of carbonaceous aerosols during pre-monsoon[17,43,44]. Such build-up of absorbing aerosols during pre-monsoon over IGP and the Himalayan slopes, and anomalous mid and upper tropospheric warming induced by these aerosols are postulated to cause anomalies in the Asian summer monsoon due to an atmospheric radiative–dynamical process proposed as elevated heat pump (EHP) effect[5,10]. Bollasina *et al.*[9] showed a link between high loads of absorbing aerosols and deficient spring-time precipitation through regression of rainfall on aerosol index (AI), and attributed it dissipation of clouds through the aerosol semi-direct effect. Also such absorbing aerosol loading contributes to enhanced melting of the Himalayan glaciers due to snow darkening and greater forcing on snow[45].

We have examined the inter-annual variability in spring-time $M_{BC}$ enhancement (Figure 6 *a*), by taking the difference between seasonal mean $M_{BC}$ from winter to spring (magnitude and percentage difference) for each of the years. An enhancement varying between 39% and 94% (~23–62 ng $m^{-3}$) has been noticed in $M_{BC}$ from winter to spring; and the highest enhancement is noticed in 2012, with the spring $M_{BC}$ (128 ± 101 ng $m^{-3}$) becoming almost double its winter value. It is worth mentioning here that the inter-annual variations in seasonal mean $M_{BC}$ for winter (or other seasons) are not as conspicuous as those seen during spring.

The potential reasons for such enhancement and its inter-annual variability could be the variations associated with changes in the source strengths and transport efficiency determined by the convection strength in individual years. For example, when the whole measurement period

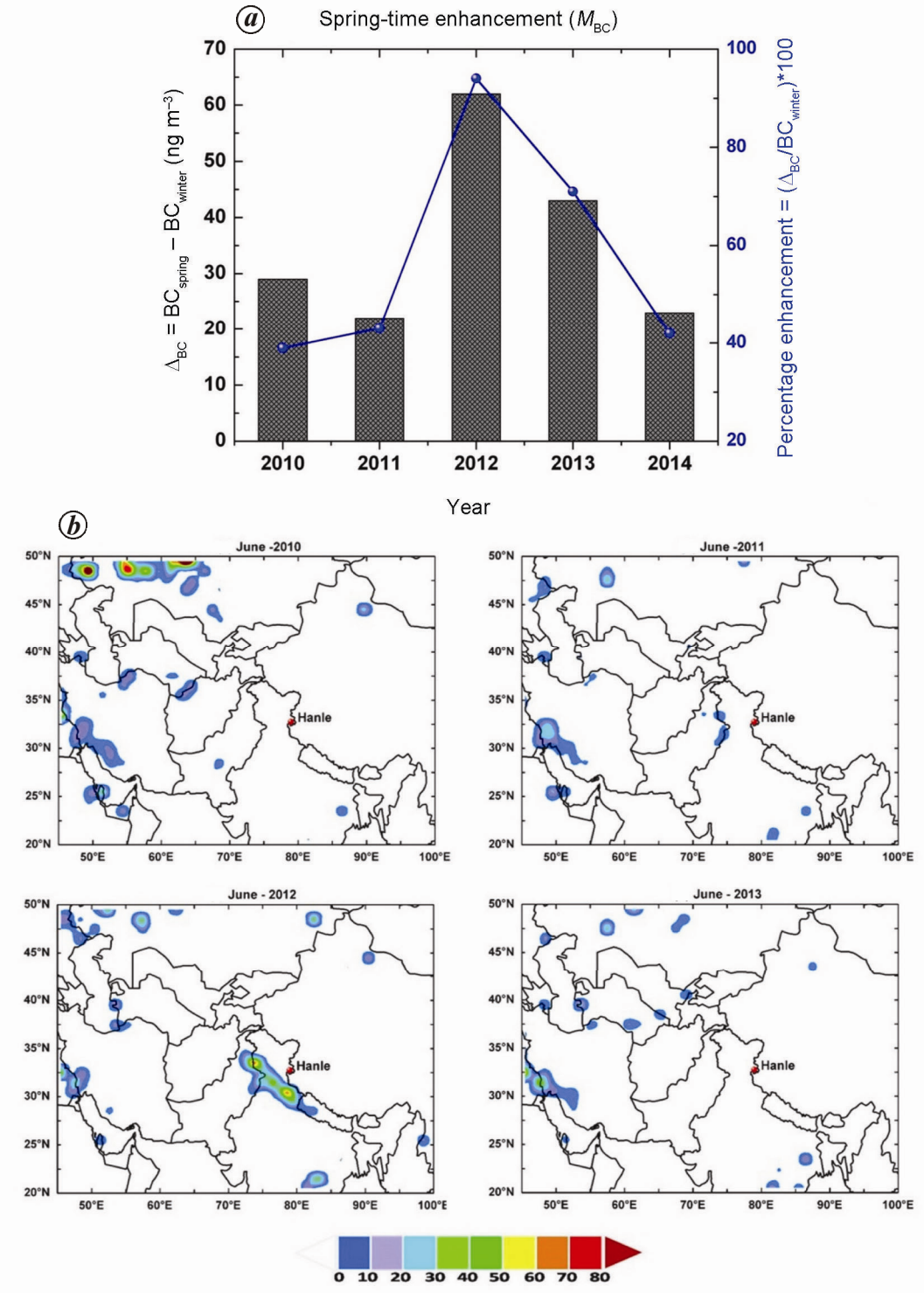


**Figure 6.** ***a***, Inter-annual variation in spring-time enhancement in $M_{BC}$ in absolute magnitude (ng m$^{-3}$) as well as percentage difference from winter to spring. ***b***, Spatial distribution of MODIS cloud-corrected fire pixel counts for June during the period 2010–2013.

is considered, June 2012 has the highest $M_{BC}$ (181 ± 140 ng m$^{-3}$; Figure 3). We examined MODIS (Moderate Resolution Imaging Spectro-radiometer) cloud-corrected fire pixel counts (monthly Climate Modeling Grid Fire Product (MOD14CMH) at a 0.5° spatial resolution) for June during the years 2010–13 (Figure 6 *b*). Noticeably higher fire counts occurrence to the west/southwest of Hanle is seen in June 2012, which is reflected in the higher $M_{BC}$ enhancement, and highlights the role of regional source strength.

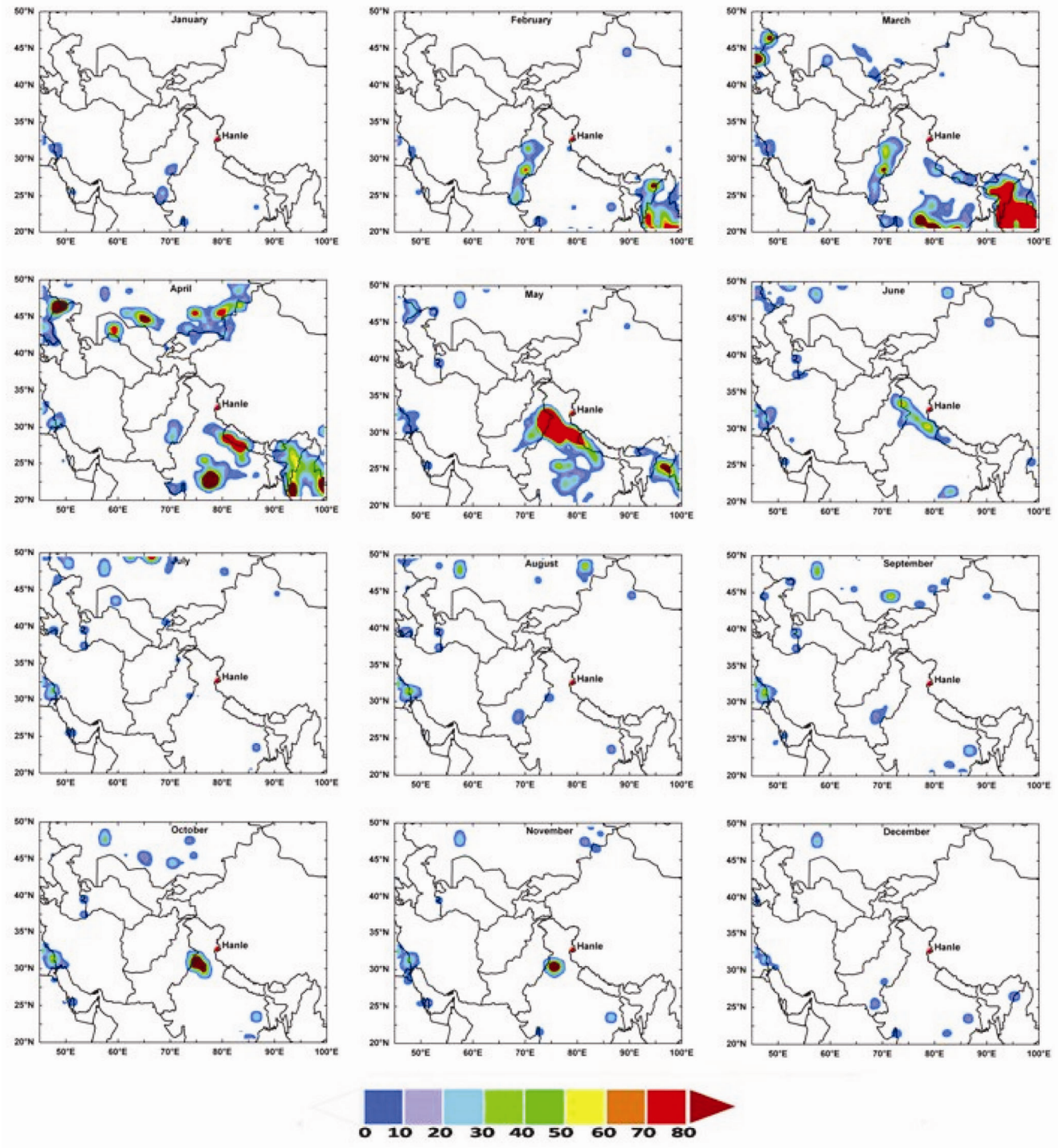


**Figure 7.** Spatial distribution of MODIS cloud-corrected fire pixel counts for all the months during 2012. Colour bar indicates the frequency count; the geographic location of Hanle is also marked in each panel.

### *Role of transport from source regions*

Further, the seasonal variation in regional sources (mainly from northwest India) contributes to the observed annual pattern of $M_{BC}$, especially to the distinct peak observed in October, a feature that has been persistent in all the years. To understand this in detail and to illustrate the seasonal features of regional sources associated with biomass burning the spatial distribution of fire counts derived from MODIS was examined. Figure 7 shows a typical spatial distribution of fire counts over India during 2012. It is clear that large areas to the west/southwest of Hanle (the northwest regions of India and the Himalayan foothills) witnessed intense burning activities during spring

months as well as in October. BC produced from these intense plumes are lifted up through convection and advected to the western Himalaya by the prevailing synoptic winds. The apparent lack of such regional sources during summer is also evident from the figure. During October, the occurrence of higher fire-count over northwest India (Punjab, Haryana) associated with intense burning activities led to the observed peak in $M_{BC}$. Interestingly, the October peak in aerosol absorption was noticeable at the NCO-P station as well (figure 4 *a* in Andrews *et al.*[42] and figure 1 *b* in Marcq *et al.*[46]). The peak in $M_{BC}$ observed during October is unique to the high-altitude locations, Hanle and NCO-P. By November, the winter conditions (sub-zero temperatures and appearance of snow caps on the mountain peaks) set in, with shallow local atmospheric boundary layer (ABL) keeping the pollutants close to the surface; and the high-altitude peaks being above this local ABL, will be free from the regional sources of BC. However, stations located at the foothills (e.g. Nainital) will continued to be exposed to the regional sources and hence the $M_{BC}$ levels continue to be high till the spring months. Earlier studies also have shown the influence of transported plumes originating from crop residue burning in the northwest India over the Himalayan sites[17,43,44,47]. Kaskaoutis *et al.*[44] attributed the high aerosol loading observed over the eastern Himalaya during post-monsoon to the possible transport of plumes originated from crop residue and biomass burning activities over the western IGP (mainly Punjab). By November, the winter conditions (sub-zero temperatures and appearance of snow caps on the mountain peaks) set in, with shallow local ABL keeping the pollutants close to the surface and with the mountain peaks being above this local ABL, BC level decreases in November.

It is worth mentioning here that the quantitative delineation of contribution from regional sources to the overall loading is difficult, but few attempts have been made by researchers in this direction. Kopacz *et al.*[48] used WRF-Chem simulations to identify the potential contributors of BC to different glaciers over the Himalaya and Tibetan plateau. Using an extensive back-trajectory analysis, Lu *et al.*[49] suggested that South Asia and East Asia contributed 67% and 17% respectively, to the BC over the Himalaya and Tibetan Plateau during 1996–2010. They also pointed out that West Asia and Europe are dominant contributors to BC loading over the northern Himalaya. Recently, Ji *et al.*[50] have simulated BC and organic carbon (OC) over the Himalayan regions using a regional climate model (RegCM4.3) coupled with a chemistry–aerosol module, and assessed the distribution, deposition and transport pathways, which highlighted contribution of the westerly winds to the transport of these species.

To examine long-range transport pathways and identify the seasonal changes in potential source regions which affect the aerosol concentrations over Hanle, concentrated weighted trajectory (CWT) analysis[26,30] was performed for surface BC mass concentrations (Figure 8). In the CWT method, observed concentration at the receptor site is assigned to the respective back trajectory, and by considering the residence time of the trajectory in each cell the weighted trajectory is distributed to an array of grid cells. It is important to note that the back trajectory suggests only a possible pathway of advection of air mass to a given region and while making scientific interpretation using back trajectories, the uncertainties involved in its calculation must be considered. In complex undulating terrain like the Himalaya, the statistical uncertainties in the back trajectory calculations can be reduced by analysing a large set of trajectories[49]. In the present study, the trajectories computed for individual days during the entire five-year period have been used to arrive at the mean picture for the different seasons, so that the errors are minimized while interpreting the CWT maps. Nevertheless, back trajectories are useful suggestive tools to identify primary transport pathways of aerosols to locations far away from the source regions. It is clear from Figure 8, that the potential source regions affecting the concentrations over Hanle are located towards its west and southwest (West Asia, the Middle East desert regions and the North African regions), whereas advection of aerosols from the IGP has remained minimal. From Figure 8 *b*, it is evident that the spring-time enhancement is due to long-range transport from these source regions. Even though Hanle is influenced by advection from the west for most part of the year, magnitude of the transport component varies from season to season. The contribution of long-range transport to $M_{BC}$ over Hanle is highest during spring (Figure 8 *b*) and lowest during winter (Figure 8 *a*). It may be seen from Figure 8 *d* that there is notable contribution from regional sources located towards west of Hanle during autumn (which is seen in the MODIS fire counts examined in earlier section), which explains the second peak in $M_{BC}$ seen in October.

### *Aerosol optical depth*

Since the surface $M_{BC}$ shows distinct annual pattern with a high in spring, to delineate whether the spring-time enhancement is confined only to the surface, seasonal changes in columnar spectral AOD were examined. The spectral AOD showed a distinct annual pattern which is repeated in all the years. Figure 9 shows the Annual variation of the long-term mean AOD at four representative wavelengths (380, 500, 750 and 1025 nm) spanning over the spectral range covered by MWR over Hanle. In general, the mean spectral AOD values vary in the range 0.01–0.30 at different wavelengths and are quite low, but there is a clear enhancement in AOD during spring (March–May) compared to other seasons; the lowest AOD values are found in winter. This feature of spring-time enhancement in AOD is consistent with the

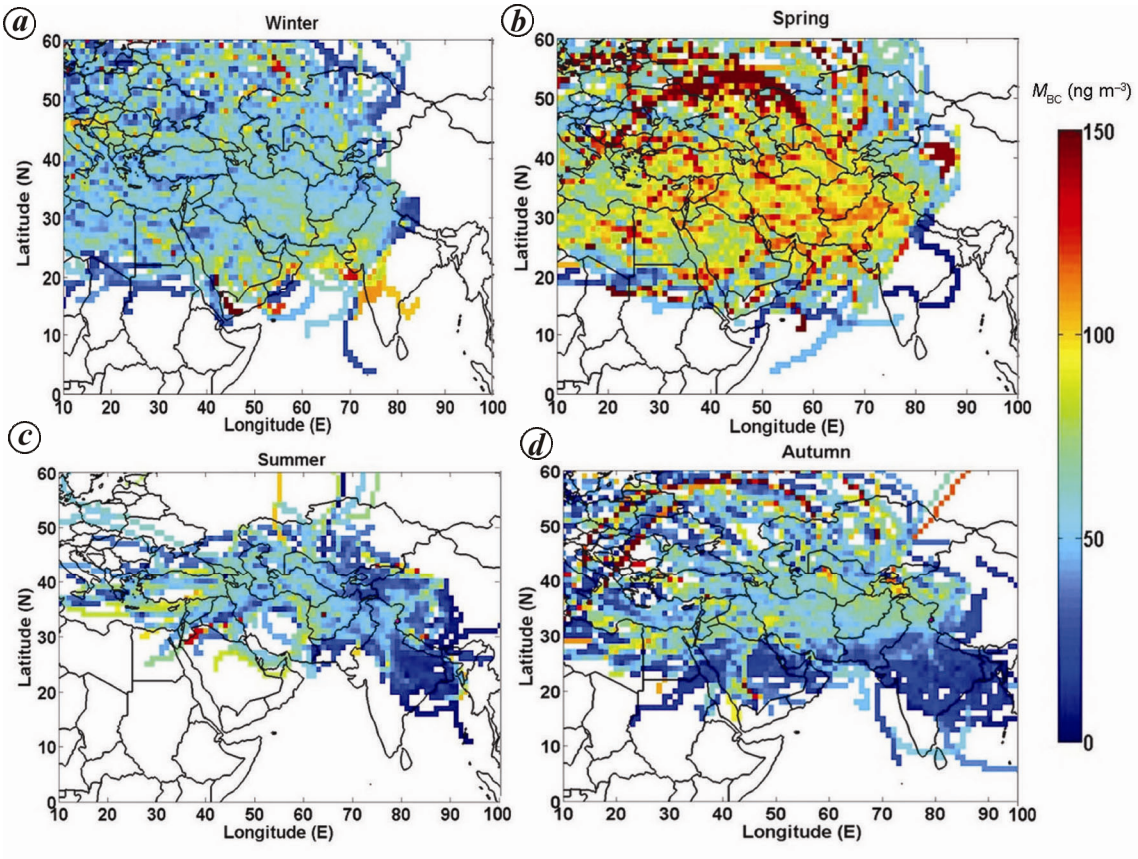


**Figure 8 *a–d*.** Concentration weighted trajectory map for $M_{BC}$ (ng m$^{-3}$) during different seasons showing potential source regions. Colour scale represents $M_{BC}$ (ng m$^{-3}$).

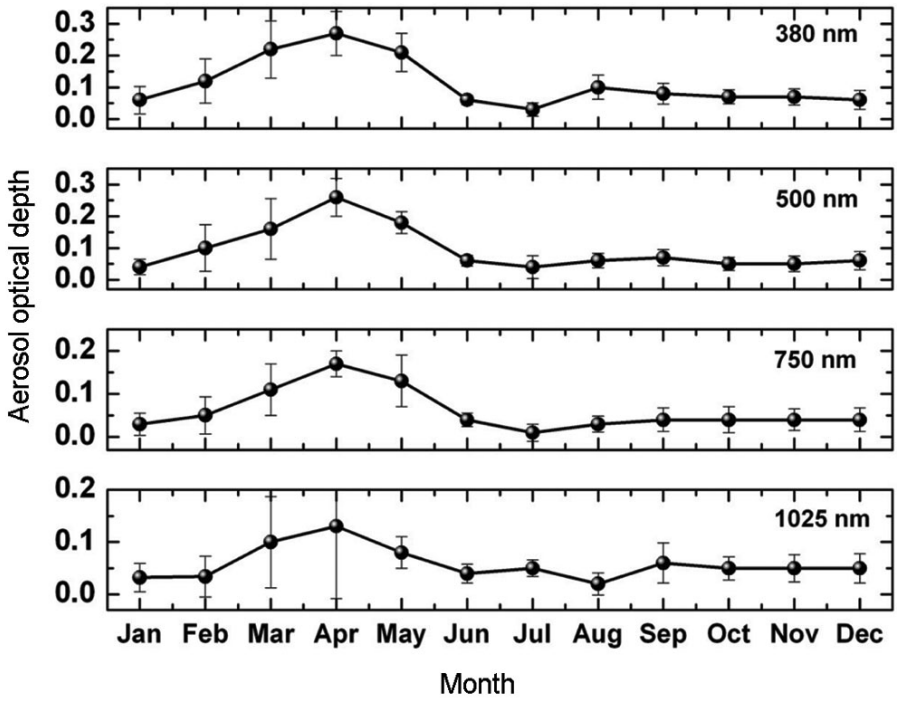


**Figure 9.** Temporal variations of monthly mean (averaged over 2009–14) aerosol optical depth over Hanle at four selected wavelengths. Vertical lines through the points represent standard deviation of the mean.

observed enhancement in near-surface BC loading. The monthly mean AOD at 500 nm varies from ~0.01 in December to ~0.13 in April, with a long-term annual mean of ~0.06 ± 0.04, which suggests the pristine nature of this location. Gobbi *et al.*[51] have reported seasonal mean AOD values varying between 0.04 and 0.08 over the high-altitude location NCO-P (5079 m amsl), while Cong *et al.*[52] have reported an annual mean AOD of ~0.05 at 500 nm over Nam Co (4720 m amsl) in the central Tibetan Plateau. Although the spring-time enhancement is observed in the surface as well as columnar aerosol properties, the magnitude of surface $M_{BC}$ at Hanle is significantly low compared to NCO-P, while the columnar AOD is higher than that is seen at NCO-P[46], which indicates the possible elevated aerosol layers over Hanle during spring.

Further, the examination of frequency of occurrence of AOD at 500 nm (not shown here) suggests that almost 90% of the values lie below 0.1. However, the higher AOD values noticed predominantly during spring, suggest seasonal changes associated with distinct aerosol sources. We have examined this further, using the spectral Angstrom exponent ($\alpha$), which revealed clear seasonal transition in aerosol types with higher $\alpha$ (~1.2) in autumn indicating fine particle contribution, and lower $\alpha$ in spring (~0.34) suggesting the dominance of coarse-mode particles, which indicate the role of transported dust. Ningombam *et al.*[28] analysed CALIOP (the Cloud–Aerosol Lidar with Orthogonal Polarization)-derived aerosol vertical profiles along with back trajectories superimposed with the MODIS fire count data and suggested that the episodes having high AOD and low $\alpha$ (mostly during spring season) were associated with the presence of desert dust at altitudes of 5–7 km amsl. The airmass trajectories during such periods mostly arrived from longer distances with relatively higher altitudes and passed over different desert regions. In case of high AOD and high $\alpha$ (>0.8) episodes, the airmasses reaching the station were highly localized (passed through densely populated and industrialized Punjab, Haryana, and the western regions to northwest India) and arrived from relatively lower altitudes, which were likely to transport anthropogenic aerosols. Gogoi *et al.*[30] have pointed out that although the near-surface accumulation-mode aerosols remained nearly steady throughout the year, the columnar abundance of fine-mode aerosols (indicated by $\alpha$) varied with season, which could be attributed to the possible presence of elevated aerosol layers at Hanle. Interestingly, there were no distinct peaks in AOD in any other season, similar to the second peak in $M_{BC}$ seen in October. Table 2 provides the seasonal mean values of $\alpha$ along with $M_{BC}$ and AOD at 500 nm.

### *Vertical distribution of aerosols*

As highlighted in the preceding sections, spring-time enhancement is seen both in the near-surface $M_{BC}$ as well as columnar AOD values over Hanle. A comparison among various Himalayan sites suggests that one of the potential causes for the observed spring-time enhancement is long-range transport with seasonal and altitudinal variations (distinct airmasses arriving at different ranges of the Himalayas) in pathways and strength. Also, comparison of observed values at Hanle (~4520 m amsl) and NCO-P (5079 m amsl) suggest that higher values of $M_{BC}$ are seen at NCO-P as well, whereas higher columnar AOD is found at Hanle during spring (importantly, the synoptic scale dynamics as well as the transport mechanisms responsible for the seasonal modulation in aerosol over both the locations are similar). This indicates the possible elevated aerosol abundance at higher altitudes during spring over Hanle. To quantify the vertical extent of the spring-time enhancement over Hanle, vertical profiles of extinction coefficient at 532 nm from CALIOP aboard the A-train satellite CALIPSO (the Cloud–Aerosol Lidar and Infrared Pathfinder Satellite Observations) level-2, version-3 data (CAL_LID_L2_05kmAPro-Prov-V3), were examined within 1° × 1° geographic grid centred at Hanle for the period between August 2009 and December 2013. The seasonally averaged extinction coefficient profiles from CALIOP were normalized with the seasonal mean AOD values obtained using MWR instrument. Cloudy profiles were screened based on the cloud aerosol discrimination (CAD) values. Figure 10 shows vertical profiles of seasonal mean extinction coefficients, that clearly highlight the presence of elevated aerosol layers (5–7 km amsl) during spring, which possibly results in the elevated AOD values. Such elevated layers are the resultant of either long-range transport and/or enhanced regional convective vertical transport of aerosols followed by their advection. The discussion in the previous section using CWT maps showed that, the potential source regions during spring are located in West Asia and the Middle East desert regions. So the elevated aerosol layers could have emanated due to long-range dust transport. Earlier investigations by Marinoni *et al.*[14,34] have suggested that during 'acute pollution events' with enhanced aerosol levels over the Indian subcontinent and the IGP region, especially during spring season, the Himalaya can be strongly influenced by the vertical upward transport of anthropogenic pollutants and mineral dust. Brun *et al.*[53], using satellite data analysis, suggested that the aerosol intrusion in Himalayan valleys due to the strong northwesterly winds above the Himalayan ridges could result in the advection of dust, mixed with fine-mode aerosol particles, and subsequently the formation of elevated aerosol layers during pre-monsoon season.

Information on enhancement in aerosol concentrations and high aerosol loading events over the Himalayan region during spring is useful to understand the aspects of EHP hypothesis, e.g. as demonstrated by Wonsick *et al.*[54], who used convection as a proxy to rainfall and reported enhanced convection and rainfall in the

**Table 2.** Seasonal mean values of $M_{BC}$, aerosol optical depth (AOD) at 500 nm and Angstrom exponent ($\alpha$) over Hanle

| Season | $M_{BC}$ (ng m$^{-3}$) | AOD at 500 nm | Angstrom exponent ($\alpha$) |
|---|---|---|---|
| Winter | 57 ± 37 | 0.05 ± 0.02 | 0.62 ± 0.05 |
| Spring | 102 ± 64 | 0.11 ± 0.08 | 0.34 ± 0.12 |
| Summer | 49 ± 40 | 0.06 ± 0.03 | 0.91 ± 0.08 |
| Autumn | 65 ± 35 | 0.04 ± 0.03 | 1.20 ± 0.06 |

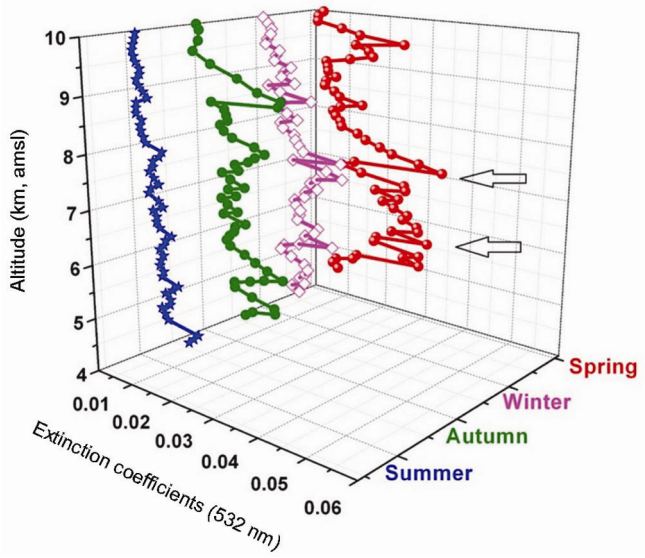


**Figure 10.** Mean vertical profiles of aerosol extinction coefficients at 532 nm during different seasons obtained from the 1° × 1° spatially resolved CALIPSO profiles (5 km aerosol profile, version-3), centred at Hanle for the period August 2009–December 2013.

Himalayan foothills during high-aerosol years (with larger AOD values). Ji *et al.*[50] have reported that, although seasonal variations in the dry deposition are not significant, the wet deposition rate of carbonaceous aerosols is greater during the non-monsoon seasons than the monsoon season in the northwest Himalayan regions. The efficient long range transport resulting in higher amounts of absorbing aerosols such as BC and dust during spring, and its subsequent deposition on snow and ice-cover, coupled with increased amounts of solar insolation during this season may have strong climate consequences, resulting in atmospheric warming, changes in surface albedo and enhancing the retreat of glaciers[8,55]. Nair *et al.*[8] showed that the diurnally averaged forcing due to snow darkening over Hanle is in the range 0.87–10.2 W m$^{-2}$ and 2.6–28.1 W m$^{-2}$ for fresh snow and aged snow respectively, which is significantly higher than the clear sky direct radiative forcing at the top of the atmosphere (1.69 W m$^{-2}$ over snow surface and –1.54 W m$^{-2}$ over sandy surface). While these forcings could lead to significant warming over the Himalaya during spring, their inter-annual variability adds to the complexity of the problem. Further studies are needed to understand the snow–albedo feedback mechanisms. The present study, highlighting the spring-time enhancement in aerosol loading over the western Himalaya, is consistent with previously reported observations regarding pre-monsoon enhancement in aerosol loading over the Himalaya and the IGP region, also suggesting that such enhancement which has significant regional climatic implications, is a large-scale phenomenon.

## Summary and conclusions

In the present work, long-term (65 months) data of aerosol $M_{BC}$ and spectral AOD carried from Hanle, a high-altitude ARFINET observatory in the western Himalayas, as part of RAWEX, have been examined for temporal variations and potential source pathways. Extremely low annual mean values of $M_{BC}$ (66 ± 51 ng m$^{-3}$) and AOD at 500 nm (0.061 ± 0.042) highlight the pristine nature of Hanle. Both $M_{BC}$ and spectral AOD show distinct annual variation with spring-time enhancement. Significant inter-annual variability is found in the spring-time enhancement of $M_{BC}$, due to varying strength of regional sources and transport. Concentrated weighted trajectory analysis for identifying contribution from long-range transport suggests maximum source strength during spring and potential source regions are located to west/southwest of the sampling location (western IGP, West Asia, the Middle East desert regions and the North African regions). Seasonal changes in the spectral dependence of AOD with Angstrom exponent ($\alpha$) varying from 0.52 to 1.2, suggest varying source characteristics and dominance of coarse-mode particles during spring. The vertical extend of elevated aerosol layers are found to be in the range 5–7 km amsl during spring from the analysis of vertical profiles of extinction coefficients from CALIPSO data.

1. IPCC, Climate Change, The Physical Science Basis. Contribution of Working Group I to the Fifth Assessment Report of the Intergovernmental Panel on Climate Change (eds Stocker, T. F. *et al.*), Cambridge University Press, Cambridge, UK, 2013, p. 1535.
2. Ramanathan, V. and Carmichael, G., Global and regional climate changes due to black carbon. *Nature Geosci.*, 2008, **1**, 221–227.
3. Jacobson, M. Z., Strong radiative heating due to the mixing state of black carbon in atmospheric aerosols. *Nature*, 2001, **409**, 695–697.
4. Ramanathan, V. *et al.*, Indian Ocean experiment: an integrated analysis of the climate forcing and effects of the great Indo-Asian

haze. *J. Geophys. Res*., 2001, **106**, 28,371–28,398; doi: 10.1029/2001JD900133.
5. Lau, K. M., Kim, M. K. and Kim, K. M., Asian summer monsoon anomalies induced by aerosol direct forcing: the role of the Tibetan Plateau. *Climate Dyn*., 2006, **26**, 855–864; doi: 10.1007/s00382-006-0114-z.
6. Vaux Jr, H. J. *et al.*, *Himalayan Glaciers: Climate Change, Water Resources, and Water Security*, National Academies Press, Washington, DC, 2012.
7. Lawrence, M. G. and Lelieveld, J., Atmospheric pollutant outflow from southern Asia: a review. *Atmos. Chem. Phys*., 2010, **10**, 11,017–11,096; doi: 10.5194/acp-10-11017-2010.
8. Nair, V. S., Babu, S. S., Moorthy, K. K., Sharma, A. K. and Marinoni, A., Black carbon aerosols over the Himalayas: direct and surface albedo forcing. *Tellus B*, 2013, **65**, 19738; http://dx.doi.org/10.3402/tellusb.v65i0.19738.
9. Bollasina, M., Nigam, S. and Lau, K. M., Absorbing aerosols and summer monsoon evolution over South Asia: An observational portrayal. *J. Climate*, 2008, **21**, 3221–3239; doi: 10.1175/2007JCLI2094.1.
10. Gautam, R., Hsu, N. C., Lau, K. M., Tsay, S. C. and Kafatos, M., Enhanced premonsoon warming over the Himalayan–Gangetic region from 1979 to 2007. *Geophys. Res. Lett.*, 2009, **36**, L07704; http://dx.doi.org/10.1029/ 2009GL037641.
11. Pant, P. *et al.*, Aerosol characteristics at a high-altitude location in central Himalayas: optical properties and radiative forcing. *J. Geophys. Res*., 2006, **111**, D17206; http://dx.doi.org/10.1029/2005JD006768.
12. Lau, K. M. *et al*., The Joint Aerosol Monsoon Experiment: a new challenge for monsoon climate research. *Bull. Am. Meteorol. Soc.*, 2008, **89**, doi: 10.1175/BAMS-89-3-369.
13. Hyvarinen, A. P., Lihavainen, H., Komppula, M., Sharma, V. P., Kerminen, V. M., Panwar, T. S. and Viisanen, Y., Continuous measurements of optical properties of atmospheric aerosols in Mukteshwar, northern India. *J. Geophys. Res.*, 2009, **114(**D08), 207; doi: 10.1029/2008JD011489.
14. Marinoni, A. *et al.*, High ozone and black carbon concentrations during pollution transport in the Himalayas: five years of continuous observations at NCO–P global GAW station. *J. Environ. Sci.*, 2013, **25**, 1618–1625.
15. Dumka, U. C. *et al.*, Characteristics of aerosol black carbon mass concentration over a high-altitude location in the Central Himalayas from multi-year measurements. *Atmos.. Res.*, 2010, **96**, 510–521.
16. Bonasoni, P. *et al.*, Atmospheric brown clouds in the Himalayas: first two years of continuous observations at the Nepal Climate Observatory-Pyramid (5079 m). *Atmos. Chem. Phys*., 2010, **10**, 7515–7531.
17. Kumar, R. *et al.*, Influences of the spring-time northern Indian biomass burning over the central Himalayas. *J. Geophys. Res.*, 2011, **116**, D19302; http://dx.doi.org/10.1029/2010JD015509.
18. Moorthy, K. K., Satheesh, S. K., Babu, S. S. and Dutt, C. B. S., Integrated campaign for aerosols, gases and radiation budget (ICARB): an overview. *J. Earth Syst. Sci.*, 2008, **117**, 243–262; doi: 10.1007/s12040-008-0029-7.
19. Satheesh, S. K., Moorthy, K. K., Babu, S. S., Vinoj, V. and Dutt, C. B. S., Climate implications of large warming by elevated aerosol over India. *Geophys. Res. Lett.*, 2008, **35(**L19), 809, doi: 10.1029/2008GL034944.22.
20. Babu, S. S. *et al.*, Free tropospheric black carbon aerosol measurements using high-altitude balloon: do BC layers build their own homes up in the atmosphere? *Geophys. Res. Lett.*, 2011, **38**(L08), 803; doi: 10.1029/2011GL046654.
21. Kotamarthi, V. R. and Satheesh, S. K., Ganges Valley Aerosol Experiment. Air & Waste Management Association. *Magazine Environ. Managers*, 2011, pp. 20–26.
22. Kotamarthi, V. R., Ganges Valley Aerosol Experiment (GVAX) Final Campaign Report, DOE/SC-ARM-14-011, 2013.
23. Moorthy, K. K., Babu, S. S., Manoj, M. R. and Satheesh, S. K., Buildup of aerosols over the Indian region. *Geophys. Res. Lett.*, 2013, **40**, 1–4.
24. Babu, S. S. *et al.*, Trends in aerosol optical depth over Indian region: potential causes and impact indicators. *J. Geophys. Res.*, 2013, **118**, 11794-11806.
25. Moorthy, K. K. *et al.*, Fine and ultra-fine particles at near free-tropospheric environment over the high-altitude station Hanle, in Trans-Himalayas: new particle formation and size distribution. *J. Geophys. Res.*, 2011, **116**, D20212; doi: 10.1029/2011JD016343.
26. Babu, S. S. *et al.*, High altitude (~4520 m amsl) measurements of black carbon aerosols over Western Himalayas: seasonal heterogeneity and source apportionment. *J. Geophys. Res.*, 2011, **116**, D24201; doi: 10.1029/2011JD016722.
27. Verma, N., Bagare, S. P., Ningombam, S. S. and Singh, R. B., Aerosol optical properties retrieved using Skyradiometer at Hanle in western Himalayas. *J. Atmos. Sol. Terres. Phys.*, 2010, **72**, 115–124; doi:10.1016/j.jastp.2009.10.016.23.
28. Ningombam, S. S., Bagare, S. P., Sinha, N., Singh, R. B., Srivastava, A. K., Larson, E. and Kanawade, V. P., Characterization of aerosol optical properties over the high-altitude station Hanle, in the trans-Himalayan region. *Atmos. Res.*, 2014, **138**, 308–323.
29. Ningombam, S. S., Bagare, S. P., Khatri, P., Sohn B. J. and Song, H. J., Estimation of aerosol radiative forcing over an aged-background aerosol feature during advection and non-advection events using a ground-based data obtained from a Prede Skyradiometer observation. *Atmos. Res.*, 2015, **164–165**, 76–83.
30. Gogoi, M. M. *et al.*, Physical and optical properties of aerosols in a free tropospheric environment: results from long-term observations over western trans-Himalayas. *Atmos. Environ.*, 2014, **84**, 262–274; http://dx.doi.org/10.1016/ j.atmosenv. 2013.11.029.
31. Kompalli, S. K., Moorthy, K. K., Babu, S. S. and Manoj, M. R., Aerosol mass size distribution and black carbon over a high-altitude location in Western Trans-Himalayas: impact of a dust episode. *Aeolian Res*., **15**, 2014, 161–168.
32. Kompalli, S. K., Babu, S. S. and Moorthy, K. K., Inter-comparison of aerosol optical depth from the multi-wavelength solar radiometer with other radiometric measurements. *Indian J. Radio Space Phys.*, 2010, **39**, 364–371.
33. Cao, J. J., Xu, B. Q., He, J. Q., Liu, X. Q., Han, Y. M., Wang, G. H. and Zhu, C. S., Concentrations, seasonal variations, and transport of carbonaceous aerosols at a remote Mountainous region in western China. *Atmos. Environ.*, 2009, **43**, 4444–4452.
34. Marinoni, A. *et al.*, Aerosol mass and black carbon concentrations, a two year record at NCO–P (5079 m, southern Himalayas). *Atmos. Chem. Phys.*, 2010, **10**, 8551–8562; doi: 10.5194/acp-10-8551-2010.
35. Zhao, S. Y., Ming, J., Sun, W. J. and Xiao, C. D., Observation of carbonaceous aerosols during 2006–2009 in Nyainqêntanglha Mountains and the implications for glaciers. *Environ. Sci. Pollut. Res*., 2013, doi: 10.1007/s11356-013-1548-6.
36. Zhao, S. Y., Ming, J., Xiao, C. D., Sun, W. J. and Qin, X., A preliminary study on measurements of black carbon (BC) in the atmosphere of northwest Qilian Shan. *J. Environ. Sci*., 2012, **24**(1), 152–159.
37. Carrico, C. M., Bergin, M. H., Shrestha, A. B., Dibb, J. E., Gomes, L. and Harris, J. M., The importance of carbon and mineral dust to seasonal aerosol properties in the Nepal Himalaya. *Atmos. Environ*., 2003, **37**(20), 2811–2824.
38. Sarkar, C., Chatterjee, A., Singh, A. K., Ghosh, S. K. and Raha, S., Characterization of black carbon aerosols over Darjeeling – a high-altitude Himalayan Station in Eastern India. *Aerosol. Air Qual. Res*., 2014, doi: 10.4209/aaqr.2014.02.0028.
39. Kundu, S. S. and Borgohain, A., BC mass concentration and AOD characteristics over Meghalaya, Shillong. ARFI & ICARB Scientific Progress Report ISRO-GBP, India, 2010, pp. 81–83.

40. Kuniyal, J. C., Aerosols climatology over the north-western Indian Himalayan region. ARFI & ICARB Scientific Progress Report, ISRO-GBP, India, 2010, pp. 93–99.
41. Kant, Y. and Dadhwal, V. K., Diurnal and seasonal variation of black carbon and aerosols over Dehradun. In Aerosol and clouds: climate change prospective, IASTA Conference, Darjeeling, 2010, vol. 19, pp. 461–462.
42. Andrews, E. *et al.*, Climatology of aerosol radiative properties in the free troposphere. *Atmos. Res.*, 2011, **102**, 365–393.
43. Vadrevu, K. P., Ellicott, E., Giglio, L., Badarinath, K. V. S., Vermote, E., Justice, C. and Lau, W. K. M., Vegetation fires in the Himalayan region – aerosol load, black carbon emissions and smoke plume heights. *Atmos. Environ.*, 2012, **47**, 241–251; http://dx.doi.org/10.1016/j.atmosenv.2011.11.009.
44. Kaskaoutis, D. G. *et al.*, Effects of crop residue burning on aerosol properties, plume characteristics and long-range transport over northern India. *J. Geophys. Res.*, 2014, **119**, 5424–5444; doi: 10.1002/2013JD021357.
45. Flanner, M. G., Zender, C. S., Hess, P. G., Mahowald, N. M., Painter, T. H., Ramanathan, V. and Rasch, P. J., Springtime warming and reduced snow cover from carbonaceous particles. *Atmos. Chem. Phys.*, 2009, **9**, 2481–2497.
46. Marcq, S. *et al.*, Aerosol optical properties and radiative forcing in the high Himalayas based on measurements at the Nepal climate observatory-pyramid site (5079 m asl). *Atmos. Chem. Phys.*, 2010, **10**, 5859–5872; doi: 10.5194/acp-10-5859-2010.
47. Sahai, S. *et al.*, Autumn-time post-harvest biomass burning in Punjab causing aerosol perturbation over Central Himalayas. AGU Fall Meeting Abstracts, 2013, vol. 1, p. 08.
48. Kopacz, M., Mauzerall, D. L., Wang, J., Leibensperger, E. M., Henze, D. K. and Singh, K., Origin and radiative forcing of black carbon transported to the Himalayas and Tibetan Plateau. *Atmos. Chem. Phys.*, 2011, **11**(6), 2837–2852.
49. Lu, Z., Streets, D. G., Zhang, Q. and Wang, S., A novel back-trajectory analysis of the origin of black carbon transported to the Himalayas and Tibetan Plateau during 1996–2010. *Geophys. Res. Lett.*, 2012, **39**, L01809.
50. Ji, Z., Kang, S., Cong, Z., Zhang, Q. and Yao, T., Simulation of carbonaceous aerosols over the Third Pole and adjacent regions: distribution, transportation, deposition and climatic effects. *Climate Dyn.*, 2014, doi: 10.1007/s00382-015-2509-1.
51. Gobbi, G. P., Angelini, F., Bonasoni, P., Verza, G. P., Marinoni, A. and Barnaba, F., Sunphotometry of the 2006–2007 aerosol optical/radiative properties at the Himalayan Nepal Climate Observatory-Pyramid (5079 m asl.). *Atmos. Chem. Phys. Discuss.*, 2010, **10**, 1193–1220; doi: 10.5194/acpd-10-1193-2010.
52. Cong, Z., Kang, S., Smirnov, A. and Holben, B., Aerosol optical properties at Nam Co, a remote site in central Tibetan Plateau. *Atmos. Res.*, 2009, **92**, 42–48.
53. Brun, J., Shrestha, P. and Barros, A. P., Mapping aerosol intrusion in Himalayan valleys using the Moderate Resolution Imaging Spectroradiometer (MODIS) and Cloud Aerosol Lidar and Infrared Pathfinder Satellite Observation (CALIPSO). *Atmos. Environ.*, 2011, **45**, 6382–6392.
54. Wonsick, M. M., Pinker, R. T. and Ma, Y., Investigation of the 'elevated heat pump' hypothesis of the Asian monsoon using satellite observations. *Atmos. Chem. Phys.*, 2014, **14**, 8749–8761; www.atmos-chem-phys.net/14/8749/2014/doi:10.5194/acp-14-8749-2014.
55. Yasunari, T. J. *et al.*, Estimated impact of black carbon deposition during premonsoon season from Nepal climate observatory-pyramid data and snow albedo changes over Himalayan glaciers. *Atmos. Chem. Phys.*, 2010, **10**, 6603–6615.

ACKNOWLEDGEMENTS. This study is carried out as a part of the Aerosol Radiative Forcing over India (ARFI) project of ISRO-GBP. We thank the Director, Indian Institute of Astrophysics, Bengaluru and staff of the Indian Astronomical Observatory – Hanle for help throughout the study. The Giovanni online data system, developed and maintained by the NASA GES DISC was used for analyses and visualizations in this study. We also thank the mission scientists and Principal Investigators for providing satellite data products used in this study.

doi: 10.18520/cs/v111/i1/117-131